N-electron valence state perturbation theory based on a density matrix renormalization group reference function, with applications to the chromium dimer and poly-p-phenylene vinylene

Sheng Guo, Mark A. Watson, Weifeng Hu, Qiming Sun, and Garnet Kin-Lic Chan[1]

Department of Chemistry, Princeton University, Princeton, New Jersey 08544, USA

The strongly-contracted variant of second order N-electron valence state perturbation theory (NEVPT2) is an efficient perturbative method to treat dynamic correlation without the problems of intruder states or level shifts, while the density matrix renormalization group (DMRG) provides the capability to tackle static correlation in large active spaces. We present a way to combine DMRG and strongly-contracted NEVPT2 (DMRG-SC-NEVPT2) through a general algorithm to compute high order reduced density matrices from DMRG wave functions. The capabilities of DMRG-SC-NEVPT2 is demonstrated on calculations of the chromium dimer potential energy curve, and the excitation energies of poly-p-phenylene vinylene (PPV).

I. INTRODUCTION

In manly non-trivial quantum chemistry applications, such as excited states, non-equilibrium geometries and transition-metal compounds, the methods based on mean-field electron interaction cannot even give qualitative descriptions. The deviation from mean-field electron interation, called electron correlation, is usually split into two parts: static or non-dynamic correlation and dynamic correlation. Static correlation is among the near-degenerate orbitals and can be effectively treated by allowing all possible distribution of electrons in these near-degenerate orbtals (active orbitals). One of the models based on active orbitals is complete active space self-consistent field (CASSCF) method. Dynamic correlation usually does not make as strong influences on electronic structure as the static correlation does. Dynamic correlation can be effectively discribed by low-level theories, such as perturbation theories (PT), configuration interaction singles (CISD) and doubles or coupled cluster theory (CC). If dynamic correlation and static correlation are both needed, such as the determination of energy order of excited states in conjugated molecules or transition metal compounds, the multi-reference (MR) versions of the theories mentioned above are needed. They are called multi-reference perturbation theories (MRPT)[1], multi-reference configuration interaction (MRCI)[2] or multi-reference coupled clusters theories (MRCC)[3].

In CASSCF and MR methods (MRPT, MRCI and MRCC) based on CASSCF wave functions, static correlation within the active orbitals is solved exactly through the full configuration interaction (FCI). The exponential increasing of computations of FCI limits the number of active orbitals. The density matrix renormalization group (DMRG)[4–9] has made it possible to employ large active spaces for electronic structure problems in quantum chemistry.[10–26] It has become straightforward to use DMRG as a robust numerical solver for static electron correlation problems. Examples of applications include benchmark solutions of small molecules[11,12,19,27], multi-center transition metal clusters[18,21,25,28], as well as molecular crystals[29]. It is a good alternative of FCI.

There were also several attempts to add dynamic correlation on the top of DMRG ansatz. For example, DMRG-CT[30], DMRG-CASPT2 [31], DMRG-cu(4)-MRCI [32] in the internal-contraction(IC) framework and MPS-PT[33], MPS-LCC [34] in fully uncontracted framework. In internal-contraction methods, high order reduced density matrices of the DMRG active space wavefunction are required. Such density matrices are simple objects in a theoretical sense, but are computationally non-trivial to obtain.

In this work, we have developed a general algorithm to efficiently compute high order reduced density matrix (RDM) from DMRG wave functions. Using these RDM calculations, we may then implement a variety of methods to treat electron correlation external to the DMRG active space. An example of this, we have implemented the second order N-electron valence state perturbation theory (NEVPT2)[35–37], an intruder-state-free multireference perturbation theory in its strongly-contracted variant, on top of the DMRG reference wavefunction, a method we call DMRG-SC-NEVPT2. To demonstrate the potential of this approach, we apply this method to study the potential energy curve of the chromium dimer, and to compute the excitation energies of the quasi-one dimensional conjugated poly(p-phenylene vinylene) (PPV). The chromium dimer is a particularly demanding small molecule that has been widely studied with many methods[31,34,38–43], and thus forms a good test bed to demonstrate the performance of DMRG-SC-NEVPT2. Using an active space with 22 orbitals and basis sets extrapolated to the CBS limit, we show that we can compute both the spectroscopic constants and the full curve, with an accuracy that compares quite favourably to earlier calculations. PPV is of interest as the prototypical light-emitting polymer[44,45]. This property relies on the correct ordering of the first optically bright 1^1B_u state and dark 2^1A_g state, which requires an appropriate description of electron correlation[46–51]. With DMRG-SC-

NEVPT2, we show that we can compute the excitation energies and energy ordering of the different states accurately starting from the full-valence active π space of the molecule.

II. THEORIES

A. DMRG wavefunction and optimization algorithm

As with other wavefunction methods in quantum chemistry, DMRG is based on a wavefunction ansatz, namely the matrix product state (MPS). An MPS is a non-linear wavefunction, built from a contraction of tensors for each orbital in the basis. If an MPS is composed of tensors with a limited dimension (called the bond dimension, M) it explores only a physically motivated, but restricted, subset of the Hilbert space. By increasing M, the MPS ansatz will then converge to the full configuration interaction (FCI) result. The DMRG algorithm provides a combination of renormalization and truncation steps that efficiently find a variational and optimal MPS. In practice, two slightly different types of MPS are used in practical DMRG calculations: the one-site and two-site MPS.

The one-site MPS is defined as

$$|\Psi\rangle = \sum_{n_1, n_2 \cdots n_p \cdots n_k} \mathbf{A}^{n_1} \mathbf{A}^{n_2} \cdots \mathbf{A}^{n_p} \cdots \mathbf{A}^{n_k} \quad (1)$$

Here, n_i is the occupancy of orbital i, one of $\{|\rangle, |\uparrow\rangle, |\downarrow\rangle, |\uparrow\downarrow\rangle\}$, and k is the number of orbitals. For a given n_i, $\mathbf{A}^{n_i}$ is an $M \times M$ matrix, except for the first and last ones; the dimensions of $\mathbf{A}^{n_1}$ and $\mathbf{A}^{n_k}$ are $1 \times M$ and $M \times 1$ respectively. This ensures that for a given occupancy string $n_1 n_2 \cdots n_k$ the $\mathbf{A}^{n_1} \mathbf{A}^{n_2} \cdots \mathbf{A}^{n_k}$ product yields a scalar, namely, the coefficient of the determinant $|n_1 n_2 \cdots n_k\rangle$.

Similarly, the two-site MPS is defined as

$$|\Psi\rangle = \sum_{n_1, n_2 \cdots n_p \cdots n_k} \mathbf{A}^{n_1} \mathbf{A}^{n_2} \cdots \mathbf{A}^{n_p n_{p+1}} \cdots \mathbf{A}^{n_k} \quad (2)$$

The only difference with the one-site MPS, is that one of the tensors ($\mathbf{A}^{n_p n_{p+1}}$) is associated with two sites at a time. The two-site MPS thus has slightly more variational freedom than the one-site MPS, and further is different depending on which sites contain the special tensor.

In the DMRG sweep algorithm, $\langle \Psi | H | \Psi \rangle$ is variationally optimized, and a single tensor (A^{n_i} for a one-site MPS or $A^{n_i, n_{i+1}}$ for a two-site MPS) is updated during the sweep at site i. This update leads to solving an eigenvalue problem of an effective "superblock" Hamiltonian, which is a $4M^2 \times 4M^2$ matrix. The multiplication between this effective Hamiltonian and a MPS is usually computed using $O(k^2)$ "normal" and "complementary" operators built from different sets (blocks) of the active orbitals. The cost of this eigenvalue problem is

$O(k^2 M^3)$ for a single tensor update, and $O(k^3 M^3)$ for a whole sweep optimization.

As discussed, a two-site MPS has more variational freedom at the site where the special tensor is placed. This allows the DMRG optimization to change quantum numbers, i.e. conserved local symmetries, during the sweep, and thus helps avoid local minima. Further, the discarded weight associated with the renormalization step in a two-site MPS sweep optimization can be used to extrapolate away the residual error due to finite bond dimension M. However, as the two-site MPS wavefunction at each step of the sweep is slightly different (because the special tensor is moved along the sweep), the two-site formalism does not provide a unique definition of the DMRG expectation values. Thus, to evaluate the reduced density matrix, we complete the DMRG sweep optimization in the one-site representation, to obtain a single DMRG wavefunction. This is referred to as the "two-site to one-site" algorithm (a two-site MPS optimization followed by a one-site one)[27]. From here on when we refer to an MPS, we will mean the one-site MPS.

B. Reduced density matrix (RDM) evaluation algorithm

High order RDM's are common in post-active space methods that are used to capture the "dynamic" correlation outside of the active space, such as multireference configuration interaction[2] and multireference perturbation theory[1,37]. The expression of quantities in terms of RDM's is a feature of the internally contracted formulations, which avoid the expansion of the external correction to the active space wavefunction explicitly in terms of many-particle basis states (such as Slater determinants or configuration state functions). Internally contracted CASPT2[1] and NEVPT2[37] (both strongly and partially contracted variants) require the four-particle RDM, while higher levels of correlation can require even higher order RDM's.

In principle, the evaluation of RDM's in DMRG is straightforward; the evaluation of a matrix element such as $\langle \Psi | a_i^\dagger a_j | \Psi \rangle$ where Ψ is an MPS, is an operation of $O(kM^3)$ cost and can be carried out within any standard DMRG implementation. However, a naive algorithm which evaluates each RDM element separately would lead to far too high a computational cost. Instead, the efficient evaluation of the RDM's of an MPS requires forming suitable DMRG renormalized operators which can be reused in *all* RDM elements $\langle a_i^\dagger a_j \rangle$. Such efficient algorithms to build the 2-RDM were proposed some years ago by several groups[52,53], and require only $O(k^3 M^3)$ cost, as opposed to the $O(k^5 M^3)$ cost arising in a naive element by element evaluation. The efficient algorithm to build the 3-RDM was introduced by Kurashige and Yanai.[31] Here we introduce a more general algorithm that automatically organises the necessary DMRG renormalized operators for any order of RDM. The RDM's we will generally be interested in will be the spin-summed

quantities, e.g. for the 2-RDM, this is

$$\gamma_{ijkl} = \sum_{\sigma,\tau} \langle\Psi| a_{i,\sigma}^\dagger a_{j,\tau}^\dagger a_{k,\tau} a_{l,\sigma} |\Psi\rangle \qquad (3)$$

1. General loop over orbital type patterns and number patterns

To organize the efficient and non-redundant evaluation of the RDM elements, we label each element in terms of two classifiers: its "type pattern" (which describes the pattern of creation and annihilation operators, ordered by the sites on the lattice), and its "number pattern" (which describes how to partition the creation and annihilation operators). The complete set of RDM elements can be then be obtained efficiently with proper reuse of intermediates in a DMRG sweep, by looping over all type patterns, and all indices corresponding to given number patterns, at each step of the sweep (with a few restrictions associated with edge cases near the ends of the sweep, described in the appendix), building the DMRG renormalized operators corresponding to the given type and number patterns, and forming the appropriate contractions with the DMRG renormalized wavefunction.

The type pattern is precisely defined as follows. Consider an RDM element $\langle a_i^\dagger a_j^\dagger \ldots a_m a_n \ldots \rangle$. We reorder the indices such that the indices of the creation and annihilation operators are arranged successively in the order as they appear in the DMRG site ordering: $\hat{o}_{i'} o_{j'} \ldots o_{m'} o_{n'}$, with $i' \le j' \le \cdots \le m' \le n'$ and where o is either a or $a^\dagger$. The corresponding binary pattern of $2N$ (where N is the rank of the RDM) creation and annihilation operators appearing in the above operator string is the type pattern of the RDM matrix element.

The number pattern encodes how to partition the labels of the expectation value in $\langle a_i^\dagger a_j^\dagger \ldots a_m a_n \ldots \rangle$ onto different blocks in the DMRG sweep, so as to maximize the reuse of DMRG renormalized operators. Recall that a DMRG sweep consists of a sequence of operations over the orbitals; at each step in the DMRG sweep, there is the set of orbitals preceding the current orbital (the system block $(\mathcal{S})$), the current orbital (the dot block $(\mathcal{D})$), and the set of orbitals whose associated site tensors have yet to be optimized (the environment block $(\mathcal{E})$). The intermediates in the construction of an RDM matrix element are DMRG renormalized operators built and stored on the three blocks. To determine the renormalized operators to build, we partition the $2N$ orbital labels of the operator $\hat{O}$ among the 3 blocks. The most efficient partitioning (when generating the full set of RDM elements) is to compute a given element from renormalized operators with the maximum number of orbital labels appearing on the dot block, and an equal number of orbital labels on the system and environment blocks. For typical RDM elements (i.e. not for elements such as γ_{0000}), at least one orbital label can be placed on D and at most $N-1$ orbital labels on E by choosing an appropriate position
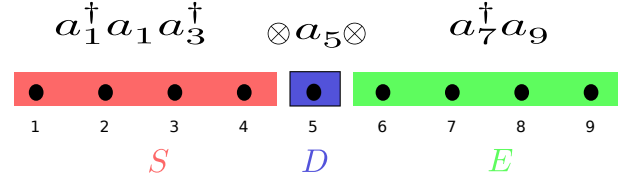

FIG. 1. Evaluation of a three RDM element $\gamma_{137;159}$. $a_1^\dagger a_1 a_3^\dagger$ is on S, a_5 is on D, and $a_7^\dagger a_9^\dagger$ is on E. It belongs to $(3,1,2)$ "number pattern" and $(a^\dagger a a^\dagger a a^\dagger a)$ "type pattern".

of the dot site (i.e. the step in the DMRG sweep). The numbers $\{n_S, n_D, n_E\}$ then denote the numbers of orbital labels distributed on the different blocks, and this is the number pattern. One can generate all valid number patterns, by considering all cases where the number of orbital labels on S is no more than N, that on D is no more than 4 and that on E is no more than $N-1$, and the total is $2N$ except for some edge cases for the first step and last step in the sweep, as discussed in the appendix. The number pattern and type pattern for a RDM element is illustrated in Fig. II B 1.

With the above process, the renormalized operators that need to be constructed on each block S, D, and E in the DMRG sweep, are enumerated by the corresponding set of type patterns and number patterns of the RDM that is being built. In total this leads to $O(k^N)$ renormalized operators that need to be built, most of which are constructed on the system block S at different steps in the sweep. The cost to build these operators is $O(k^N M^3)$ at each step of the sweep and $O(k^{N+1} M^3)$ in total.

2. Computing the expectation values

After building the renormalized operators needed on the three blocks, $[O]^S$, $[O]^D$, $[O]^E$ at site i of the sweep, they are traced with the renormalized DMRG wavefunction, i.e. the site tensor $\mathbf{A}^{n_i}$. This corresponds to the computation

$$\gamma = \sum_{snes'n'e'} A_{se}^{n_i} p[O]_{ss'}^S [O]_{nn'}^D [O]_{ee'}^E A_{s'e'}^{n_i'} \qquad (4)$$

where the above tensor contraction is performed in stages (e.g. contracting s, n, e indices separately) and intermediates like $\sum_{snes'n'e'} A_{se}^{n_i} [O]_{ss'}^S A_{s'e'}^{n_i'}$ are reused to minimize the computational cost, and p is a parity operation that inserts appropriate minus signs for fermions[11]. The total cost of this step for the N-RDM is $O(k^{N+1} M^3 + k^{2N} M^2)$.

3. Spin recoupling

Through the above steps, an expectation value such as $\langle a_0^\dagger a_1^\dagger a_2 a_3 \rangle$ is obtained. For a non-spin-adapted DMRG

algorithm, where $a^\dagger, a$ are simple creation and annihilation operators, we can then obtain γ_{0132} by permuting a_2 and a_3 with appropriate signs. For spin-adapted DMRG implementations, the $a^\dagger, a$ are spin tensor creation and annihilation operators, and $\langle a_0^\dagger a_1^\dagger a_2 a_3 \rangle$ is a reduced matrix element which generates multiple density matrix values through the Wigner-Eckhart theorem. The elements generated correspond to $\langle \{[(a_0^\dagger a_1^\dagger)_{\mathcal{S}}^{S_1}(a_2)_{\mathcal{D}}]^{S_2}(a_3)_{\mathcal{E}}\}^{S_3} \rangle$ with different spins S_1, S_2, S_3. The spin tensor creation and annihilation operators can be expanded as a linear combination of spin orbital creation and annihilation operators, leading to a set of linear equations to obtain the spin orbital RDM elements from a single spin reduced matrix element. Using singlet embedding[22,54], expectation values for the spin tensor combinations with non-zero total spin are zero, significantly decreasing the number of expectation values to compute. The coefficients appearing in the linear equations are the same for all operators with the same pattern and can thus be generated automatically and reused. The cost of this process is independent of the DMRG bond dimension M, and is thus negligible compared to the other parts of the RDM calculation.

C. N-electron valence state perturbation theory

We now briefly review the strongly contracted NEVPT2[36,37], a second-order multireference perturbation theory. The target zeroth-order wave function is defined as

$$P_{CAS}HP_{CAS}|\Psi^{(0)}\rangle = E^{(0)}|\Psi^{(0)}\rangle \tag{5}$$

where P_{CAS} is the projector onto the CAS space. The zeroth order Hamiltonian is chosen in the form given by Dyall[55]:

$$H^D = H_i + H_v + C \tag{6}$$

where H_i is a one-electron (diagonal) operator in the nonactive (core and external) subspace:

$$H_i = \sum_{i,\sigma}^{core} \epsilon_i a_{i,\sigma}^\dagger a_{i,\sigma} + \sum_{r,\sigma}^{virt} \epsilon_r a_{r,\sigma}^\dagger a_{r,\sigma} \tag{7}$$

and ϵ_i and ϵ_r are orbital energies; H_v is a two-electron operator confined to the active space:

$$H_v = \sum_{ab,\sigma}^{act} h_{ab}^{eff} a_{a,\sigma}^\dagger a_{b,\sigma} + \sum_{abcd,\sigma,\eta}^{act} \langle ab|cd\rangle a_{a,\sigma}^\dagger a_{b,\eta}^\dagger a_{d,\eta} a_{c,\sigma} \tag{8}$$

where $h_{ab}^{eff} = h_{ab} + \sum_i^{core}(2\langle ai|bi\rangle - \langle ai|ib\rangle)$; and C is a constant to ensure that H^D is equivalent to the full Hamiltonian within the CAS space.

The zeroth order wave functions external to the CAS space are referred to as the "perturber functions". A perturber function is written as $|\Psi_{l,\mu}^{(k)}\rangle$. It belongs to a CAS space is denoted $P_{S_l^{(k)}}$, where k is the number of electrons promoted to ($k > 0$) or removed from ($k < 0$) the active space, l denotes the occupancy of nonactive orbitals and μ enumerates the various perturber functions in $S_l^{(k)}$. In strongly contracted NEVPT2, only one perturber function for each $S_l^{(k)}$ subspace is used. The perturber function is defined as $|\Psi_l^{(k)}\rangle = S_l^{(k)} H |\Psi^{(0)}\rangle$, where $P_{S_l^{(k)}}$ is the projector onto the space. The energy of the perturber function is

$$E_l^{(k)} = \frac{\langle \Psi_l^{(k)}| H^D |\Psi_l^{(k)}\rangle}{\langle \Psi_l^{(k)}|\Psi_l^{(k)}\rangle} \tag{9}$$

The zeroth order Hamiltonian then becomes

$$H_0 = \sum_{kl} |\Psi_l^{(k)'}\rangle E_l^{(k)} \langle \Psi_l^{(k)'}| + |\Psi^{(0)}\rangle E^{(0)} \langle \Psi^{(0)}| \tag{10}$$

where $|\Psi_l^{(k)'}\rangle$ corresponds to the normalized $|\Psi_l^{(k)}\rangle$.

The bottleneck in SC-NEVPT2 is the evaluation of the energies of the perturber functions, where up to the 4RDM appears. This 4RDM is subsequently contracted with two electron integrals in the active space to form auxiliary matrices.[37] Computing the 4RDM requires $O(k^8 M^2 + k^5 M^3)$ cost, much higher than that of a standard DMRG energy optimization. To minimize the cost, it is generally necessary to evaluate the 4RDM using a lower bond dimension than is used in the DMRG energy optimization of $|\Psi^{(0)}\rangle$. To obtain an MPS approximation of lower bond dimension for the reference, we "compress" the converged reference MPS of a larger bond dimension. This is in practice by carrying out a "reverse schedule" set of sweeps in a DMRG code, where M is decreased[27]. All of our DMRG-SC-NEVPT2 calculations use reference MPS that have been compressed in this way to compute the RDM's. The compressed bond dimension is denoted M'.

Further, to avoid storage problems in our implementation of DMRG-SC-NEVPT2, the 4-RDM is computed on the fly. In principle, it is possible to completely avoid generating the 4-RDM by directly computing the auxiliary matrices (i.e. with the integrals already contracted). This is the approach taken, for example, in Kurashige and Yanai's original implementation of DMRG-CASPT2 [31], where the auxiliary matrices can be computed with a cost scaling similar to that of the 3-RDM, using special kinds of DMRG renormalized operators as intermediates. However, the Dyall Hamiltonian in NEVPT2 involves all the active-space two-electron integrals, and this is more complicated to handle than the diagonal Fock energies that appear in the CASPT2 zeroth Hamiltonian (in its canonical representation). Although the scaling of such an algorithm may be lower, it is complicated to implement and the computational prefactor is large due to the many different intermediates that need to be considered. We have implemented such an algorithm only in

our reference NEVPT2 code that uses CASCI type reference wavefunctions, and not in our DMRG-SC-NEVPT2 code.

III. APPLICATIONS

A. Chromium dimer

The chromium dimer has been a challenging molecule for quantum chemistry for many years. This is because a relatively large active (12e, 12o) space is needed to describe the minimal spin-recoupling of the electrons involved in the nominal sextuple bond, while, at the same time, a large amount of dynamic correlation is required even to yield a bound potential energy curve.[31,34,38,40,41,56–58]

The minimal (12e,12o) CAS derived from the 3d and 4s atomic orbitals, has been widely employed in earlier chromium dimer calculations.[34,40,41,56–58] Although these earlier calculations could reproduce the general shape of the potential energy curve, they also have a number of shortcomings. For example, both CASPT2[56–58] and NEVPT2[36] based on the CASSCF(12e,12o) reference function tend to significantly overestimate the dissociation energy of the molecule, especially when large basis sets (e.g. those including g-, h-, or even i- type functions) are used.[39,40] Further, with NEVPT3,[40] starting from the CAS(12e,12o) wavefunction results in a large correction to the NEVPT2 result and an unreasonable potential energy curve. These various results suggest that (at least when used with low-orders of perturbation theory and internally contracted formulations which have a limited ability to relax the reference) the minimal (12e,12o) CAS is too small for a quantitative description.

Further, when using CASPT2, the results are also sensitive to the choice of the zero-order Hamiltonian and the level shift employed.[39,42] This is especially true for the (12e,12o) active space, but sensitivity can still be seen even in DMRG-CASPT2 calculations with a CAS(12e,28o) derived from the 3d, 4s, 4p, 4d atomic orbitals. While the DMRG-CASPT2 curves are generally close to the experimentally derived curve, the different choices of zeroth-order level shifts still yielded a variation in D_e of about 0.2 eV.[31] Since NEVPT2 does not require level shifts to avoid intruders, the above provides further incentive to compute the chromium dimer potential energy curve using DMRG-SC-NEVPT2, and with a large active space.

For our DMRG-SC-NEVPT2 calculations, we used the suite of cc-pwcVXZ (X = T,Q,5) basis sets. No basis set superposition error (BSSE) corrections were applied due to the large basis sets used (which included h- and i-type functions). The X2C Hamiltonian was used to describe scalar relativistic effects. The DMRG reference and corresponding RDM and DMRG-SC-NEVPT2 calculations were performed using the BLOCK program[22]. All other calculations were done in PYSCF[59]. In the figures, the
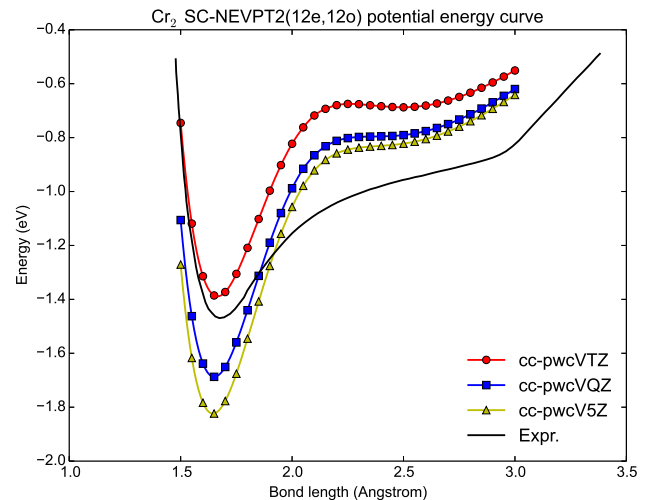

FIG. 2. NEVPT2(12e,12o) potential energy curve with a suite cc-pwcVXZ (X=T,Q,5) basis set

energy of the isolated atoms is set as zero.

We first show the SC-NEVPT2(12e,12o) potential energy curve of Cr_2 in Figure 2 to demonstrate the basis set convergence with the cc-pwCVXZ bases. The (12e,12o) active space was obtained from a CASSCF calculation. We find that using larger basis sets together with this small active space indeed yields far too deep a curve, in agreement with earlier studies using atomic natural orbital (ANO) basis sets.[40]

We then extended the (12e,12o) active space by adding another set of σ, π, π', δ, δ' orbitals and their corresponding anti-bonding orbitals to obtain a (12e,22o) active space. We selected the orbitals from the converged (12e,12o) CASSCF calculation based on symmetry and the orbital energies, and the orbitals were further optimized using DMRG-CASSCF (M=1000, no frozen core). Although the additional active orbitals contained both $4p$ and $4d$ orbitals at first, the optimized additional active orbitals were mainly $4d$ orbitals. This is not surprising, as a $4d$ double shell is well known to greatly improve the transition metal CAS results[60]. From the DMRG-CASSCF optimized orbitals, we then carried out a final larger DMRG calculation with M=4000 to obtain an accurate reference wavefunction. The resulting DMRG reference energy in the active space is accurate to better than 0.1 mE_h. To compute the RDM's for the DMRG-SC-NEVPT2 calculation, the large bond dimension reference MPS was compressed down to an MPS with M'=800. Finally, the (TZ/QZ/5Z) energies were extrapolated to the complete basis set (CBS) limit using an exponential formula for the DMRG-CASSCF energy, and an l^{-3} formula for DMRG-NEVPT2 correction energy, where l is the maximum angular momentum of basis set.

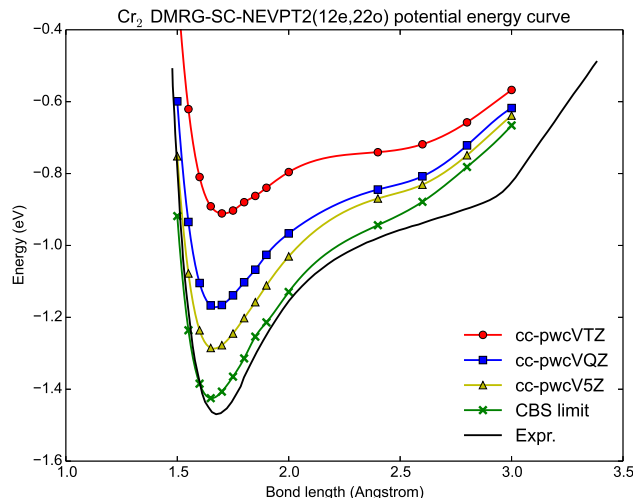Figure 3 shows the potential energy curves obtained with the cc-pwcVXZ (X=T,Q,5) basis sets and the X2C

FIG. 3. DMRG-SC-NEVPT2(12e,22o)(M=800) potential energy curve with a suite of cc-pwcVXZ (X=T,Q,5) basis sets, and the extrapolated CBS limit. The experimental curve is taken from Ref. 61.

TABLE I. Spectroscopic constants for the ground state of Cr_2 using different methods.

	$D_e(eV)$	$R_0(Å)$	$\omega_e(cm^{-1})$
DMRG-SC-NEVPT2(12e,22o) [a]			
M=800	1.425	1.654	482
M=1200	1.429	1.656	471
DMRG-CASPT2(12e,28o)[b]	1.610	1.681	480
MR-AQCC(12e,12o)[c]	1.355	1.685	459
FP-AFQMC[d]	1.63(5)	1.65(2)	552(93)
experiment	1.47(5)[e]	1.679[f]	480.6(5)[e]
	1.47 ±0.1 [g]		

[a] It is from the fitting of the energies at five points R=1.60,1.65, 1.70, 1.75, and 1.80 Å
[b] DMRG-CASPT2(12e,28o)/$g_1(M = \infty)$ with cc-pwcV5Z basis set in Ref. 31
[c] TZP/QZP CBS limit in Ref. 41
[d] Ref. 62
[e] Ref. 61
[f] Ref. 63
[g] Ref. 64

Hamiltonian, as well as the extrapolated CBS curve. A comparison of the CBS curve to curves obtained with other methods is shown in Fig. 4. We see that larger basis sets using this active space yield systematically improved curves, and that the CBS potential energy curve agrees very well with the experimental curve, over a wide range of distances. The only significant deviation occurs near the strong bend at about 2.8Å, where the reliability of the RKR potential has previously been questioned.[38] The spectroscopic constants are shown in Table I. Our obtained CBS D_e of 1.43eV is very close to the results from Casy and Leopoid's negative ion photoelectron spectroscopy, 1.47eV[61], while the bond-length and vibrational frequency also agree well. It is remarkable to note that even with the largest cc-pwcV5Z basis, the binding energy is still 0.14 eV away from the CBS limit, demonstrating the very large basis set effects in this system.

Compared to earlier "accurate" calculations, the computed DMRG-SC-NEVPT2 curve here compares quite favourably. For example, near the equilibrium distance, the DMRG-SC-NEVPT2(12e,22o) curve is almost identical to the DMRG-CASPT2(12e,28o) curve[31]. However, in the stretched $4s$ bonding ("shoulder") region, the DMRG-SC-NEVPT2(12e,22o) curve is much closer to the experimental one. This seems consistent with the increased correlation strength in the $4s$ bonding region, which should be harder to describe with the simpler zeroth order Hamiltonian employed in CASPT2. Across the full range of distances, the DMRG-SC-NEVPT2 curve also appears considerably more accurate than the MR-AQCC(12e,12o) curve, likely due to the larger active space employed.

The (12e,28o) CAS used in the earlier DMRG-CASPT2 calculations contained $4p$ orbitals. However,

the accuracy of the DMRG-SC-NEVPT2(12e,22o) curve as compared to the DMRG-CASPT2(12e,28o), together with the fact that only $4d$ orbitals remain in the active space after orbital optimization, suggest that $4d$ orbitals are more important than the $4p$ orbitals in the correlations of this system. It has also been suggested in some studies that semi-core correlations (involving the $3s$, and $3p$ orbitals) are also very important in this system. In Fig. 5 we show the corresponding curves computed using as (28e,20o) active space containing the semi-core $3s, 3p$ orbitals and $3d, 4s$ valence shell (but no $4d$ shell). We see that the curves are much worse than the curves obtained with the (12e,22o) active space above. This suggests that the double shell correlations are more important than the semi-core correlations in this system, and that the latter are well accounted for at the second-order perturbation theory level.

B. Poly(p-phenylene vinylene)

Poly(p-phenylene vinylene) is a well-known light emitting conjugated polymer. It has several low-lying states that participate in its photophysics and has been extensively investigated with many theoretical methods, for example the semi-empirical methods[46], DMRG based on Pariser-Parr-Pople (PPP) model Hamiltonian[47,48,51], time-dependent density functional theory[49] and symmetry-adapted cluster configuration interaction (SAC-CI)[50]. Our DMRG-SC-NEVPT2 provides a new approach for the prediction of excitation energy of low-lying states. Limited by the computations of DMRG-SC-NEVPT2, it is not feasible for very long ppv chains. We only use PPV3 (three phenyl rings) as an example to demonstrate the capability of DMRG-SC-NEVPT2 for low-lying excited states in conjugated molecules.

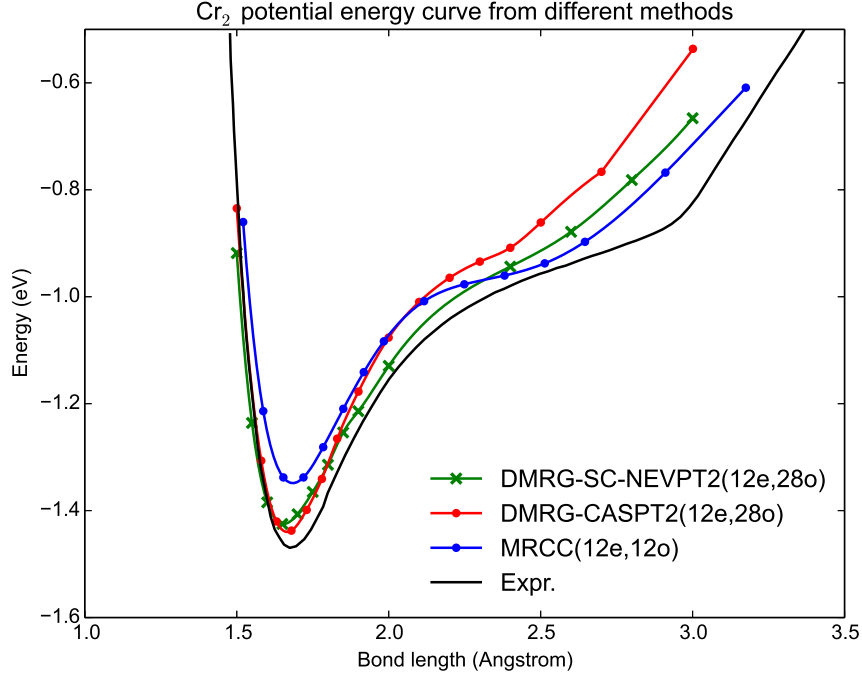The cc-pVDZ basis set and a (22e,22o) active space

FIG. 4. Cr_2 potential energy curves from different methods. The DMRG-CASCPT2(12e,28o) curve is from Ref. 31 and the MR-AQCC(12e,12o) curve is from Ref. 41.
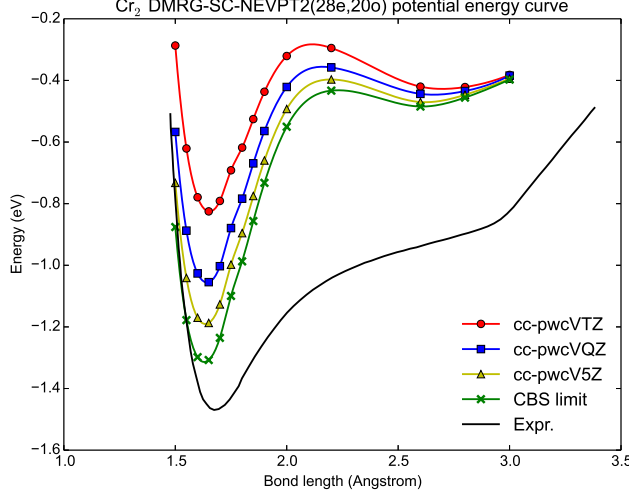

FIG. 5. DMRG-SC-NEVPT2(28e,20o)(M=800) potential energy curve with a suite of cc-pwcVXZ (X=T,Q,5) basis sets, and the extrapolated CBS limit. The experimental curve is taken from Ref. 61.

containing the 22 conjugated π, π^* orbitals were used. The ground state equilibrium geometry of PPV3 was obtained via DMRG-CI geometry optimization[65], which is implemented within an interface between Block and ORCA[66], starting from a guess from the DFT/B3LYP optimized geometry. The DMRG-CI geometry optimization was first run at $M=1000$, and near convergence with $M=2000$. Canonical Hartree-Fock orbitals were used in the DMRG calculations in the geometry optimization.

Compared to canonical orbitals, localized orbitals usually give a better convergence for DMRG calculation.[27] Therefore, further state-averaged DMRG-CI calculations were carried out for 6 lowest singlet states, based on split-localized orbitals (localize the occupied and unoccupied π, $\pi*$ orbitals separately with Pipek-Mezey method[67]). The energies were convergied to $0.2mEh$ with a bond dimension, 3200. The excited states were identified according to their excitation signature from the ground state, through transition 1RDM and 2RDM in canonical Hartree-Fock orbitals. And the symmetry of states are determined by the symmetry of excitation signature: excitation between two orbitals of different symmetries leads to B_u symmetry, and excitation between two orbital of same symmetry leads to A_g symmetry. Due to the lack of $\pi - \sigma$ interactions, the energy order of excitations states are qualitatively different with previous experimental or theoretical results[48,51]. The state with a HOME→LUMO excitation signature did not have the lowest excitation energies.

Then, the $\pi - \sigma$ interactions were included through DMRG-SC-NEVPT2 theory. The MPS wave functions from DMRG-CI calcualtions were compressed with smaller bond dimensions, 500 and 750. The difference in excitation energy induced by different bond dimen-

TABLE II. Comparisons of vertical excitation energy in vacuum from different methods

State	DMRG-SC-NEVPT2	DMRG/PPP	SAC-CI	expt
1^1B_u	3.86	3.52^a, 3.91^b, 3.751^c,	3.57^d	3.69^e
2^1A_g	4.66	4.06^a, 4.618^c		

[a] Ref. 47
[b] Ref. 48
[c] Ref. 51
[d] Ref. 50
[e] Ref. 68

sions in the DMRG-SC-NEVPT2 calculation is less than $0.6 meV$ (Table III). The error from incomplete renormalized basis in DMRG can be ignored in the prediction of excitation energies.

The excitation energy of first bright state predicted by DMRG-SC-NEVPT2 agrees well with the experimental data[68] (Table II). And according to our calculations, there is a B_u state, besides the first bright state, underlying the $2A_g$ state.

IV. CONCLUSION

In this work, we described an efficient and general algorithm to compute high order RDM's from a DMRG wave function. These RDM's may be used as the starting point for many kinds of internally contracted dynamic correlation methods. Using up to the 4th order RDM, we combined DMRG and strongly contracted NEVPT2 to obtain an intruder state free second order multireference perturbation theory that can be used with large active spaces.

To demonstrate the capability of the DMRG-SC-NEVPT2 method, we calculated the potential energy curve of the chromium dimer and the excited states of PPV3. For the chromium dimer, the extended active space included $4d$ orbitals and the so called "double d" shell. Our obtained curve compares quite favourably with earlier calculations and tracks the experimental curve very closely, except at very bond-lengths where the experimental inversion may be suspect. For PPV3, using an active space containing the full set of π, π^* orbitals, we found that the dynamic correlation included through NEVPT2 allowed us to obtain a reasonable ordering of the low-lying excited states, and the lowest excitation energy in good agreement with the experimental data. In summary, these examples paint an optimistic picture for the potential of applying the DMRG-SC-NEVPT2 methodology to a wide range of challenging problems.

APPPENDIX A: EDGE CASES FOR NUMBER PATTERNS IN RDM

All number patterns in the N-RDM, $\{n_\mathcal{S}, n_\mathcal{D}, n_\mathcal{E}\}$, need to be computed if

$$0 \leq n_\mathcal{S} \leq N \tag{11}$$

$$0 \leq n_\mathcal{E} \leq N - 1 \tag{12}$$

$$1 \leq n_\mathcal{D} \leq 4 \tag{13}$$

$$n_\mathcal{S} + n_\mathcal{D} + n_\mathcal{E} = 2N \tag{14}$$

However, there are some RDM elements, whose indices cannot be arranged as described above, because too many their indices lie in first or last site. We need additional number patterns to compute these elements.

For the first step of the DMRG sweep, additional patterns are added. These patterns satisfy

$$N + 1 \leq n_\mathcal{S} \leq \min(4, 2N) \tag{15}$$

$$0 \leq n_\mathcal{D} \leq 4 \tag{16}$$

$$n_\mathcal{S} + n_\mathcal{D} + n_\mathcal{E} = 2N \tag{17}$$

For the last step of the DMRG sweep, additional patterns are also added. These patterns satisfy

$$N \leq n_\mathcal{E} \leq \min(4, 2N) \tag{18}$$

$$0 \leq n_\mathcal{D} \leq 4 \tag{19}$$

$$n_\mathcal{S} + n_\mathcal{D} + n_\mathcal{E} = 2N \tag{20}$$

Because $\mathcal{S}$ (or $\mathcal{E}$) is composed of single site in the first or last step of sweeping, expectation value of an operator with more than two a or two $a^\dagger$ is zero. The number of indices on single sites should not be more than 4.

APPPENDIX B: RESTRICTION ON TYPE PATTERNS

It is a waste of resources to compute RDM elements which are zero or redundant. And RDM elements can be computed through multiple types of combinations of operators. We implemented some restrictions to skip calculations for zero and redundant RDM elements.

The operators a_i and $a_j^\dagger$ are permuted, so the orbitals indices not decrease. Only the permutation between two operators with different orbital indices are needed. If a_i precedes $a_j^\dagger$ and $i = j$, the compound operators are not needed in the RDM calcualtion. For a single site block, the type with a ahead of $a^\dagger$ is omitted. For other blocks, the loop over $o_i o_j o_k \ldots$ should satisfy $i \leq j \leq k \ldots$ ('=' is only valid when the two adjacent operators in normal order).

Further the RDM (but not transition RDM) is a Hermitian matrix. Using 3-RDM as an example

$$\langle a_i^\dagger a_j^\dagger a_k^\dagger a_l a_m a_n \rangle = \langle (a_i^\dagger a_j^\dagger a_k^\dagger a_l a_m a_n)^\dagger \rangle = \langle a_n^\dagger a_m^\dagger a_l^\dagger a_k a_j a_i \rangle \tag{21}$$

TABLE III. Excitation energy (eV) calculated from DMRG-SC-NEVPT2 with localized orbitals. The transition signature is calculated DMRG-CI wave function with M= 750. The excitation coefficient of the transition $i \rightarrow j$ ($i, j \rightarrow k, l$) is given by $\langle \Psi | a_j^\dagger a_i | 1^1 A_g \rangle$ ($\langle \Psi | a_l^\dagger a_k^\dagger a_j a_i | 1^1 A_g \rangle$). And the transition labels $n \rightarrow m'$ are interpreted as follows: 1, 2, 3 ... denote HOMO, HOMO-1, HOMO-2 ... canonical orbitals, while $1'$, $2'$, $3'$ ... denote LUMO, LUMO+1, LUMO+2 canonical orbitals.

Symmetry	excitation signature	M=500	M=750	DMRG-CI(M=3200)
$1^1 B_u$	$(1 \rightarrow 1')$	3.8628	3.8625	5.1311
$2^1 B_u$	$0.71\ (5 \rightarrow 1') + 0.66\ (1 \rightarrow 3')$	4.4980	4.4978	4.4952
$2^1 A_g$	$0.49\ (2 \rightarrow 1') + 0.42\ (1 \rightarrow 2')$	4.6634	4.6634	4.8454
	$+\ 0.47\ (1, 1 \rightarrow 1', 1')$			
$3^1 B_u$	Too many terms	4.8268	4.8262	4.7541
$4^1 B_u$	Too many terms	4.8441	4.8443	4.7571

We can always use transpose and permutation to make the operators begin with $a^\dagger$ rather than a (the first operator of the list is the operator with the smallest orbital index). Therefore, all type patterns begining with a list are omitted.

Similarly, if an operator begins with $a_i^\dagger a_i$, $a_i^\dagger a_i a_j^\dagger a_j$ or $a_i^\dagger a_i a_j^\dagger a_j a_k^\dagger a_k$, the remaining set of operators also has the transpose and permutation symmetry. e.g.:

$$
\begin{aligned}
&\langle a_i^\dagger a_i (o_j o_k \dots) \rangle \\
=&\langle (a_i^\dagger a_i (o_j o_k \dots))^\dagger \rangle \\
=&\langle (o_j o_k \dots)^\dagger (a_i^\dagger a_i)^\dagger \rangle \\
=&\langle a_i^\dagger a_i (o_j o_k \dots)^\dagger \rangle
\end{aligned}
\tag{22}
$$

where $i < j \leq k \dots$

Therefore, there is no need to compute the type patterns in which a follows $a_i^\dagger a_i$.

[1] K. Andersson, P. A. Malmqvist, B. O. Roos, A. J. Sadlej, and K. Wolinski, J. Phys. Chem. **94**, 5483 (1990).
[2] R. J. Buenker and S. D. Peyerimhoff, Theor. Chim. Acta **35**, 33 (1974).
[3] N. Oliphant and L. Adamowicz, J. Chem. Phys. **94**, 1229 (1991).
[4] S. R. White, Phys. Rev. Lett. **69**, 2863 (1992).
[5] S. R. White, Phys. Rev. B **48**, 10345 (1993).
[6] S. Östlund and S. Rommer, Phys. Rev. Lett. **75**, 3537 (1995).
[7] S. Rommer and S. Östlund, Phys. Rev. B **55**, 2164 (1997).
[8] U. Schollwöck, Rev. Mod. Phys. **77**, 259 (2005).
[9] U. Schollwck, Annals of Physics **326**, 96 (2011), january 2011 Special Issue.
[10] S. R. White and R. L. Martin, J. Chem. Phys. **110**, 4127 (1999).
[11] G. K.-L. Chan and M. Head-Gordon, J. Chem. Phys. **116**, 4462 (2002).
[12] O. Legeza, J. Röder, and B. A. Hess, Phys. Rev. B **67**, 125114 (2003).
[13] G. Moritz and M. Reiher, J. Chem. Phys. **126**, 244109 (2007).
[14] F. Verstraete, V. Murg, and J. I. Cirac, Adv. Phys. **57**, 143 (2008).
[15] K. H. Marti, I. M. Ondík, G. Moritz, and M. Reiher, J. Chem. Phys. **128**, 14104 (2008).
[16] D. Zgid and M. Nooijen, J. Chem. Phys. **128**, 14107 (2008).
[17] K. H. Marti and M. Reiher, Zeitschrift für Phys. Chemie Int. J. Res. Phys. Chem. Chem. Phys. **224**, 583 (2010).
[18] Y. Kurashige and T. Yanai, J. Chem. Phys. **130**, 234114 (2009).
[19] H.-G. Luo, M.-P. Qin, and T. Xiang, Phys. Rev. B **81**, 235129 (2010).
[20] G. K.-L. Chan and S. Sharma, Annu. Rev. Phys. Chem. **62**, 465 (2011).
[21] K. H. Marti and M. Reiher, Phys. Chem. Chem. Phys. **13**, 6750 (2011).
[22] S. Sharma and G. K.-L. Chan, J. Chem. Phys. **136**, 124121 (2012).
[23] S. Wouters, P. A. Limacher, D. V. Neck, and P. W. Ayers, J. Chem. Phys. **136**, 134110 (2012).
[24] S. Wouters, N. Nakatani, D. Van Neck, and G. K.-L. Chan, Phys. Rev. B **88**, 75122 (2013).
[25] Y. Kurashige, G. K.-L. Chan, and T. Yanai, Nat. Chem. **5**, 660 (2013).
[26] S. Wouters, T. Bogaerts, P. V. D. Voort, V. V. Speybroeck, and D. V. Neck, J. Chem. Phys. **140**, 241103 (2014).
[27] R. Olivares-Amaya, W. Hu, N. Nakatani, S. Sharma, J. Yang, and G. K.-L. Chan, J. Chem. Phys. **142**, 34102 (2015).
[28] S. Sharma, K. Sivalingam, F. Neese, and G. K.-L. Chan, Nat. Chem. **6**, 927 (2014).
[29] J. Yang, W. Hu, D. Usvyat, D. Matthews, M. Schtz, and G. K.-L. Chan, Science **345**, 640 (2014).
[30] E. Neuscamman, T. Yanai, and G. K.-L. Chan, Int. Rev. Phys. Chem. **29**, 231 (2010).
[31] Y. Kurashige and T. Yanai, J. Chem. Phys. **135**, 94104 (2011).
[32] M. Saitow, Y. Kurashige, and T. Yanai, J. Chem. Theory Comput. **11**, 5120 (2015).
[33] S. Sharma and G. K.-L. Chan, J. Chem. Phys. **141**, 111101 (2014).
[34] S. Sharma and A. Alavi, J. Chem. Phys. **143**, 102815 (2015).
[35] C. Angeli, R. Cimiraglia, S. Evangelisti, T. Leininger, and J.-P. Malrieu, J. Chem. Phys. **114**, 10252 (2001).
[36] C. Angeli, R. Cimiraglia, and J.-P. Malrieu, Chem. Phys. Lett. **350**, 297 (2001).
[37] C. Angeli, R. Cimiraglia, and J.-P. Malrieu, J. Chem. Phys. **117**, 9138 (2002).
[38] B. O. Roos, Collect. Czechoslov. Chem. Commun. **68**, 265 (2003).
[39] P. Celani, H. Stoll, H.-J. Werner, and P. Knowles, Molecular Physics **102**, 2369 (2004).
[40] C. Angeli, B. Bories, A. Cavallini, and R. Cimiraglia, J. Chem. Phys. **124**, 54108 (2006).
[41] T. Müller, J. Phys. Chem. A **113**, 12729 (2009).
[42] F. Ruipérez, F. Aquilante, J. M. Ugalde, and I. Infante, J. Chem. Theory Comput. **7**, 1640 (2011).
[43] Y. Kurashige, Mol. Phys. **112**, 1485 (2014).
[44] J. H. Burroughes, D. D. C. Bradley, A. R. Brown, R. N. Marks, K. Mackay, R. H. Friend, P. L. Burns, and A. B. Holmes, Nature **347**, 539 (1990).
[45] R. H. Friend, R. W. Gymer, A. B. Holmes, J. H. Burroughes, R. N. Marks, C. Taliani, D. D. C. Bradley, D. A. D. Santos, J. L. Brédas, M. Lögdlund, and W. R. Salaneck, Nature **397**, 121 (1999).
[46] D. Beljonne, Z. Shuai, R. H. Friend, and J. L. Brédas, J. Chem. Phys. **102**, 2042 (1995).
[47] M. Y. Lavrentiev, W. Barford, S. J. Martin, H. Daly, and R. J. Bursill, Phys. Rev. B **59**, 9987 (1999).
[48] A. Shukla, Phys. Rev. B **65**, 125204 (2002).
[49] Y.-K. Han and S. U. Lee, J. Chem. Phys. **121**, 609 (2004).

[50]B. Saha, M. Ehara, and H. Nakatsuji, J. Phys. Chem. A **111**, 5473 (2007).

[51]R. J. Bursill and W. Barford, J. Chem. Phys. **130**, 234302 (2009).

[52]D. Ghosh, J. Hachmann, T. Yanai, and G. K.-L. Chan, J. Chem. Phys. **128**, 144117 (2008).

[53]D. Zgid and M. Nooijen, J. Chem. Phys. **128**, 144115 (2008).

[54]W. Tatsuaki, Phys. Rev. E **61**, 3199 (2000).

[55]K. G. Dyall, J. Chem. Phys. **102**, 4909 (1995).

[56]K. Andersson, B. O. Roos, P. A. Malmqvist, and P. O. Widmark, Chem. Phys. Lett. **230**, 391 (1994).

[57]B. O. Roos and K. Andersson, Chem. Phys. Lett. **245**, 215 (1995).

[58]B. O. Roos, K. Andersson, M. P. Flscher, P.-. Malmqvist, L. Serrano-Andrs, K. Pierloot, and M. Merchn, "Multiconfigurational perturbation theory: Applications in electronic spectroscopy," in *Advances in Chemical Physics* (John Wiley & Sons, Inc., 2007) pp. 219–331.

[59]Q. Sun, "`http://http://sunqm.github.io/pyscf`,".

[60]K. Andersson and B. O. Roos, Chem. Phys. Lett. **191**, 507 (1992).

[61]S. M. Casey and D. G. Leopold, J. Phys. Chem. **97**, 816 (1993).

[62]W. Purwanto, S. Zhang, and H. Krakauer, J. Chem. Phys. **142**, 064302 (2015).

[63]V. E. Bondybey and J. H. English, Chem. Phys. Lett. **94**, 443 (1983).

[64]C.-X. Su, D. A. Hales, and P. B. Armentrout, Chem. Phys. Lett. **201**, 199 (1993).

[65]W. Hu and G. K.-L. Chan, J. Chem. Theory Comput. **11**, 3000 (2015).

[66]F. Neese, Wiley Interdiscip. Rev. Comput. Mol. Sci. **2**, 73 (2012).

[67]J. Pipek and P. G. Mezey, J. Chem. Phys. **90**, 4916 (1989).

[68]J. Gierschner, H.-G. Mack, L. Lüer, and D. Oelkrug, J. Chem. Phys. **116**, 8596 (2002).